J Optim Theory Appl (2015) 167:761–779
DOI 10.1007/s10957-015-0778-9

Optimal Reactive Power Allocation in Large-Scale Grid-Connected Photovoltaic Systems

Zhongkui Wang[1] · **Kevin M. Passino**[1] · **Jin Wang**[1]

Received: 24 May 2013 / Accepted: 29 June 2015 / Published online: 10 July 2015

Abstract In this paper, an optimal strategy is proposed for the reactive power allocation in large-scale grid-connected photovoltaic systems. Grid-connected photovoltaic systems with direct current to alternating current inverters are able to supply active power to the utility grid as well as reactive power. The active power, extracted by the direct current to alternating current inverters, is usually controlled to be around the maximum power point of the photovoltaic array attached to it. For large-scale grid-connected photovoltaic systems with multiple direct current to alternating current inverters, due to the limited apparent power transfer capability of each inverter, the reactive power needs to be allocated among the direct current to alternating current inverters in a proper way. The proposed method achieves the maximum reactive power transfer capability of the entire system by applying classic Lagrange multiplier method. The sufficient conditions of the optimal reactive power allocation strategy are provided and mathematically proved. The proposed optimal reactive power allocation strategy is then tested in a case study against a sample large-scale grid-connected photovoltaic system.

Communicated by David G. Hull.

✉ Zhongkui Wang
wang.1231@osu.edu

Kevin M. Passino
passino@ece.osu.edu

Jin Wang
wang@ece.osu.edu

[1] Department of Electrical and Computer Engineering, The Ohio State University, 2015 Neil Ave, 205 Dreese Lab, Columbus, OH 43210, USA

Keywords Grid-connected photovoltaic systems · Lagrange multiplier · Reactive power allocation · Smart grid · Smart inverters

Mathematics Subject Classification 49M37 · 90C30 · 90C90

1 Introduction

In the current power grid, the control of voltage levels, which allows active power to be transferred, is accomplished by controlling the generation, absorption, and flow of reactive power [1]. Traditional reactive power generation units consist of capacitor banks, Static Var Compensators (SVC), and STATic COMpensators (STATCOM) [2]. In order to plan these reactive power generation units in an effective and efficient way, many optimization techniques have been employed to conquer the allocation and control challenges. For instance, the conventional methods include linear programming (LP), nonlinear programming (NLP), and mixed-integer nonlinear programming (MINLP; the intelligent approaches include simulated annealing (SA), evolutionary algorithms (EA), genetic algorithms (GA) [2].

In the future smart grid, distributed generation (DG) will provide a large amount of active power generation and participate in reactive power generation as well. Among all of the distributed generation resources, grid-connected photovoltaic (PV) electricity and energy generation systems have a significant increase worldwide. At the end of 2013, the worldwide total capacity of installed solar PV systems reached 139 GW [3]. These installed PV energy conversion systems contain a large portion of large-scale grid-connected PV systems, which are being developed to hundreds of MW level [4]. The largest installed large-scale grid-connected PV plant in the world is the Agua Caliente Solar Project in Arizona, USA, with an installed capacity of 247 MW, and it will be built to have a total capacity of 397 MW. There are also large-scale PV plants with larger capacity that are under construction, such as the Desert Sunlight Solar Farm (550 MW) in Riverside County, California, USA, the Topaz Solar Farm (550 MW) in San Luis Obispo County, California, USA, the Golmud Solar Park (200 MW installed, 370 MW being constructed) in Qinghai, China. In large-scale grid-connected PV systems, due to the limited efficiency and power conversion capability of a single PV panel, multiple PV panels are connected together in series to form a PV string, and multiple PV strings are connected in parallel to form a large PV array. The connection to the utility grid of large-scale PV plants is realized by inverters. Typical centralized PV inverters in MW-level grid-connected PV systems have a power rating under 500 kW, and some PV inverters with large capacity may have a power rating up to 700 kW [5,6]. One centralized PV inverter cannot handle the connection of the entire PV system with the grid in MW-level large-scale grid-connected PV systems. Hence, several inverters are connected in parallel, as the interface between the large-scale PV system and the utility grid [5–8].

The new topology of large-scale grid-connected PV systems imposes new challenges on existing active power generation of large-scale PV systems, as well as reactive power generation. For instance, nonuniform solar irradiation would lead to multiple peaks of the large-scale PV array's power–voltage (P–V) curve [9], and tra-

ditional maximum power point tracking (MPPT) methods lead a failure to seek the maximum power point (MPP) of the entire system. Hence, distributed control techniques were developed to solve the multiple-peak problem under the partially shading condition by applying multiple direct current to direct current (DC–DC) converters inside the PV array, such that each converter is able to guarantee the maximum active power of the PV string connected to it [10]. Additional problems associated with active power control of grid-connected PV systems have been also discussed. In [11], a dynamic programming (DP) optimization approach is used to minimize the cost of peak-shaving service of the grid-connected PV systems with energy storage elements, and the structure of a power supervisor based on an optimal predictive power scheduling algorithm is also proposed. Although certain standards [12] do not permit inverter-based DGs to regulate local voltage currently, more and more research has been focusing on reactive power generation of DGs with smart inverters, especially grid-connected PV systems. A variety of literature such as [13–15] addresses the control and optimization problems of reactive power for gird-connected PV systems with a single direct current to alternating current (DC–AC) inverter. In [13], several reactive power control methods and different PV inverters' working modes to support reactive power have been compared. Different challenges of reactive power control by PV inverters are discussed in [14], and control schemes associated with the problems are presented. In [15], an online optimal control strategy to minimize the energy losses of grid-connected PV inverters is proposed. A decentralized nonlinear autoadaptive controller is designed for such an objective. Corresponding to the distributed control techniques for the active power of large-scale PV systems, a similar approach has been also applied to the reactive power control for large-scale grid-connected PV systems, i.e., inside a large-scale grid-connected PV system, and multiple DC–AC inverters are used for the connection of PV strings with the grid. In [16], a distributed cooperative control algorithm is developed to regulate the real and reactive power outputs of multiple PV generators in a distribution network. Although the capacity of large-scale grid-connected PV systems is tremendously increased and new inverter topologies have been proposed, the reactive power generation, allocation, and control problems in the MW-level large-scale PV systems with multiple PV inverters have not been studied much.

In this paper, we propose an optimization strategy for the reactive power allocation of a system with multiple PV inverters. Under such an optimal allocation strategy, these PV inverters intend to cooperatively provide reactive power support to the grid, while simultaneously achieving maximum power transfer capability of the entire system. We provide the analytical form of the allocation strategy and mathematically prove the strategy is optimal by using optimization tools. We develop the optimal strategy for reactive power allocation into an algorithm and test such an algorithm in a case study.

2 Real and Reactive Power of Grid-Connected PV Systems

Consider a grid-connected PV system with $m \in \mathbb{N}_+$ DC–AC inverters. For each inverter, there is one PV string connected to the utility grid through it. Let the con-

tinuous variable $Q_i \in \mathbb{R}$, $i \in \{1, \ldots, m\}$, be the amount of reactive power of the ith DC–AC inverter. Suppose that $\sum_{i=1}^{m} Q_i = Q_D$, where Q_D is the reactive power demand of the utility grid, which is known. Here, we define positive Q_D to be the reactive power that the grid-connected PV systems supply to the grid and negative Q_D to be the reactive power that the grid-connected PV systems absorb from the grid.

2.1 Grid-Connected PV Systems

Let us consider one single DC–AC inverter with the PV string connected to it, as shown in Fig. 1. In Fig. 1, the PV string is connected to the utility grid through the three-phase DC–AC inverter. We assume that there is a MPPT control for the PV string. Due to the DC–AC inverter, the system shown in Fig. 1 is able to supply not only active power, but also reactive power to the utility grid. As we do not focus on the circuit level of such a system, we assume the inverter is ideal; i.e., there is no power loss on it. We also assume that the PV array generates the maximum power to the grid, and the system is able to supply/absorb reactive power to/from the grid because of the DC–AC inverter. Figure 1 only shows one inverter in the gird-connected PV systems. Now we consider the entire grid-connected PV system with multiple DC–AC inverters. The system topology diagram is shown in Fig. 2.

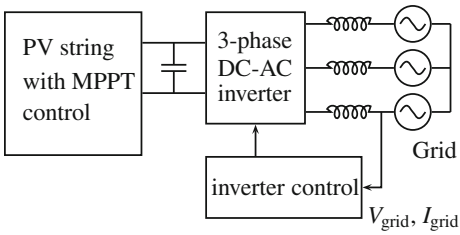

Fig. 1 System diagram of the grid-connected PV systems with one single DC–AC inverter

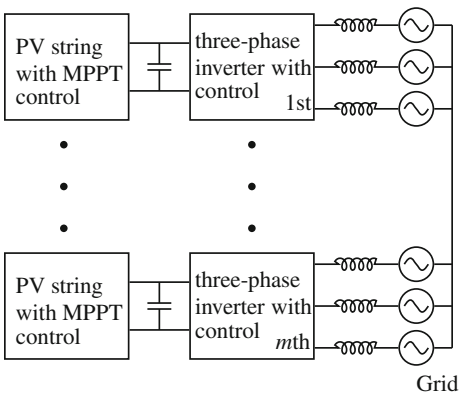

Fig. 2 System diagram of the grid-connected PV systems with multiple DC–AC inverters

2.2 Real and Reactive Power Capability Functions

Consider the ith DC–AC inverter in the system shown in Fig. 2. The inverter has limited capability to transfer real and reactive power. Suppose that $C_i^{\mathrm{LMT}} > 0$ is a constant, that we use to represent the current limit of the ith inverter. We assume that the size of the ith DC–AC inverter is optimally designed; i.e., the value of C_i^{LMT} is optimally selected based on the rating of the active power of the PV string attached to the ith inverter, such that the ith inverter does not have much additional current margin. Such design for the ith inverter reduces cost, but it makes the power transfer capability of the ith inverter limited. Let $|V| > 0$ denote the line-to-neutral voltage magnitude of the grid voltage, and $|V|$ is usually known. Let s_i be the power transfer capability function for the ith inverter, which is expressed as

$$s_i = C_i^{\mathrm{LMT}} - \frac{\sqrt{P_i^2 + Q_i^2}}{3|V|}, \tag{1}$$

where the term $\sqrt{P_i^2 + Q_i^2}/(3|V|)$ stands for the current of the ith inverter and P_i is the active power generated by the PV array. It is obvious that the current of the inverter cannot exceed the limit C_i^{LMT}. This requires the capability function $s_i \geq 0$. In (1), the capability function s_i actually calculates the current margin of the ith inverter; i.e., how much more current the inverter is able to take. Hence, (1) provides a method to define the power transfer capability of the ith inverter. As the PV array is connected to the grid through the DC–AC inverter, the active power transferred by the inverter is assumed to be at the MPP of the PV array. Another candidate capability function is

$$s_i = \frac{\sqrt{P_i^2 + Q_i^2}}{3|V|C_i^{\mathrm{LMT}}}. \tag{2}$$

The capability function in (2) represents the ratio between the inverter current and the current limit, which is similar to the one given by (1). In this paper, we use (1) to show our results (by using (2), we would obtain similar results).

2.3 Reactive Power Allocation for the Grid-Connected PV Systems

In Fig. 2, there are a total number of m DC–AC inverters that are capable of transferring real and reactive power to the grid. The total power capability function is defined as

$$s_T := \sum_{i=1}^{m} s_i = \sum_{i=1}^{m} \left(C_i^{\mathrm{LMT}} - \frac{\sqrt{P_i^2 + Q_i^2}}{3|V|} \right). \tag{3}$$

In (3), s_T represents the total current margin of the entire system. As P_i is the MPP of the ith PV string, which is known; we need to seek an optimal allocation method for Q_i, $i \in \{1, \ldots, m\}$, such that the total power capability of the system is maximized.

As discussed above, since the power capability function s_i needs to be nonnegative and $|V|$ and C_i^{LMT} are positive constants, we have

$$\sqrt{P_i^2 + Q_i^2} - 3|V|C_i^{\mathrm{LMT}} \leq 0,\ i = 1, \ldots, m. \tag{4}$$

The value of the ith inverter's reactive power Q_i can be both positive and negative. Positive Q_i means the ith inverter is providing reactive power to the grid, and a negative value of Q_i means it is absorbing the reactive power from the grid. So we can expand (4) as

$$\begin{aligned} Q_i - \sqrt{9|V|^2(C_i^{\mathrm{LMT}})^2 - P_i^2} \leq 0,\ i = 1, \ldots, m \\ -\sqrt{9|V|^2(C_i^{\mathrm{LMT}})^2 - P_i^2} - Q_i \leq 0,\ i = 1, \ldots, m. \end{aligned} \tag{5}$$

Clearly, (5) gives the upper and lower bounds of $Q_i, i = 1, \ldots, m$. If the replacements of $Q_i = -Q_i$ and $Q_D = -Q_D$ are made, then the analysis of $Q_D > 0$ is same as $Q_D < 0$, only except for sign convention. Hence, we simplify the problem by only considering the analysis of the positive part. Combining the reactive power balance equation $\sum_{i=1}^{m} Q_i = Q_D$, the reactive power allocation problem is formulated as follows,

$$\begin{aligned} \min \left[-s_T = -\sum_{i=1}^{m} \left(C_i^{\mathrm{LMT}} - \frac{\sqrt{P_i^2 + Q_i^2}}{3|V|} \right) \right] \\ \text{s.t. } h(Q) = \sum_{i=1}^{m} Q_i = Q_D \\ g_i(Q_i) = Q_i - \sqrt{9|V|^2(C_i^{\mathrm{LMT}})^2 - P_i^2} \leq 0,\ i = 1, \ldots, m. \end{aligned} \tag{6}$$

3 Optimal Reactive Power Allocation Strategy

In (6), the total reactive power generated by all the DC–AC inverters is equal to the grid demand Q_D. Hence, the allocation strategy of the reactive power for those inverters partially depends on Q_D. Moreover, (5) shows the limits, i.e., upper and lower bounds, of the reactive power of the ith inverter Q_i. Now let us consider two cases.

3.1 Optimal Allocation Strategy for Small Reactive Power Demand

For relatively small reactive power demand Q_D, we assume that the optimally allocated reactive power $Q_i^*, i = 1, \ldots, m$, satisfies (5). Next theorem provides values for the so-called relatively small reactive power demand Q_D, and if the reactive power demand of the grid satisfies the values, then the optimal allocation strategy given by the theorem applies.

Theorem 3.1 *For $i = 1, \ldots, m$, the reactive power profile*

$$Q_i^* = \frac{P_i}{\sum_{i=1}^m P_i} Q_D \tag{7}$$

is the optimal reactive power allocation strategy of (6), whenever Q_D satisfies

$$\max_{i=1,\ldots,m} \left\{ \frac{Q_i^{\min}}{P_i} \sum_{i=1}^m P_i \right\} \le Q_D \le \min_{i=1,\ldots,m} \left\{ \frac{Q_i^{\max}}{P_i} \sum_{i=1}^m P_i \right\}, \tag{8}$$

where $Q_i^{\min} = -\sqrt{9|V|^2 (C_i^{\mathrm{LMT}})^2 - P_i^2}$ and $Q^{\max} = \sqrt{9|V|^2 (C_i^{\mathrm{LMT}})^2 - P_i^2}$.

As indicated by Theorem 3.1, when (8) holds, the optimal reactive power of the ith inverter is proportional to its active power. The power capability function of the entire system s_T is

$$s_T = \sum_{i=1}^m C_i^{\mathrm{LMT}} - \frac{\sqrt{\left(\sum_{i=1}^m P_i\right)^2 + Q_D^2}}{3|V|}. \tag{9}$$

If we replace Q_D by u, then the optimal cost parameterized by u is $s_T(u)$ that is given by (9). Then, the gradient of $s_T(u)$, $\nabla s_T(u)$, is the negative of the Lagrange multiplier parameterized by u; i.e., $\nabla p(u) = -\lambda(u)$. The Lagrange multiplier is the gradient of the optimal cost function with respect to the level of the constraint.

3.2 Optimal Allocation Strategy for Large Reactive Power Demand

When (8) does not hold, we say that the reactive power demand Q_D is "relatively large." Obviously, we cannot use Theorem 3.1 to find the optimal reactive power for each inverter. For this case, the optimal reactive power of some inverters will reach the limits. To find the optimal reactive power allocation strategy for this case, we need to know which inverters' reactive power will reach the limits. Then, we have the following theorem.

Lemma 3.1 *With $Q_D > 0$ suppose there are $r \in \mathbb{N}_+$, $r \le m$, inverters with reactive power Q_i that hits the upper bound $Q_i^{\max}$; then, these inverters are the first r inverters in the order that*

$$\frac{Q_1^{\max}}{P_1} \le \frac{Q_2^{\max}}{P_2} \le \cdots \le \frac{Q_m^{\max}}{P_m}, \tag{10}$$

where

$$r = \arg\min \left\{ r : \frac{P_i}{\sum_{i=r+1}^m P_i} \left(Q_D - \sum_{i=1}^r Q_i^{\max} \right) < Q_i^{\max},\ i = r+1, \ldots, m \right\}. \tag{11}$$

Based on Lemma 3.1, we have the optimal allocation strategy for the reactive power when the reactive power demand Q_D does not satisfy (8).

Theorem 3.2 *If (8) does not hold, with $Q_D > 0$ suppose all the inverters are in the order given in (10), and there are $r \in \mathbb{N}_+$, $r < m$, inverters with reactive power Q_i that hits the upper bound; then, for $i = 1, \ldots, m$, the reactive power profile*

$$\begin{aligned} Q_i^* &= Q_i^{\max},\ i = 1, \ldots, r, \\ Q_i^* &= \frac{P_i}{\sum_{i=r+1}^{m} P_i}\left(Q_D - \sum_{i=1}^{r} Q_i^{\max}\right),\ i = r+1, \ldots, m, \end{aligned} \tag{12}$$

is the optimal reactive power allocation strategy of (6);

Theorem 3.2 indicates that if the reactive power demand Q_D does not satisfy (8), then the optimal reactive power profile will make some inverters' reactive powers hit their limits and, for other inverters, that the reactive power do not reach the limits; the optimal strategy will allocate the reactive power to be proportional to the active power.

4 Implementation: Algorithm and Case Study

In this section, we will apply the optimal reactive power allocation strategy proposed in Sect. 3 for a sample grid-connected PV system. First, we introduce an optimal reactive power allocation algorithm for grid-connected PV systems; then, we provide a sample grid-connected PV system and test the algorithm against it in simulation.

4.1 Algorithm for Optimal Reactive Power Allocation

The optimal reactive power allocation strategy proposed above is developed into an algorithm as follows:

1. Evaluate if (8) holds.
2. If (8) holds, then the reactive power of all the inverters is calculated by (7).
3. If (8) does not hold (it means the reactive power of some inverters reaches the limits), then sort all the inverters in the order given by (10).
   (a) The reactive power of the first inverter in the new order is $(Q_{1'}^{\max})$.[1]
   (b) For $i = 2' \ldots, m'$, evaluate

$$Q_D - \sum_{j=1'}^{i-1} Q_j \le \min_{j=i,\ldots,m'} \left\{ \frac{Q_j^{\max}}{P_j} \sum_{j=i}^{m'} P_j \right\}. \tag{13}$$

[1] The subscript $1'$ means it is the first inverter in the new order.

Table 1 Data of the inverters in the sample grid-connected PV system

	Type 1 inverter	Type 2 inverter
Maximum output power	250 kW	100 kW
Nominal output voltage	480 V	480 V (AC, line to line)
Nominal output current	301 A	121 A
Nominal output frequency	60 Hz	60 Hz
Number of inverters	30	25

(c) If (13) holds, then

$$Q_i = \frac{P_i}{\sum_{j=i}^{m'} P_j}\left(Q_D - \sum_{j=1'}^{i-1} Q_j\right). \tag{14}$$

(d) If (13) does not hold, then $Q_i = Q_i^{\max}$.

4.2 Case Study

In order to validate the optimal reactive power allocation algorithm, we will compare the algorithm we presented above with algorithms based on an even allocation strategy to show its optimality.

Now consider a 10 MW grid-connected PV system with two types of DC–AC inverters included. The required data of these inverters for the case study are shown in Table 1. In this system, we have a total of $m = 55$ of DC–AC inverters. Assume that for $i = 1, \ldots, 30$, $C_i^{\mathrm{LMT}} = 301$ A and $C_i^{\mathrm{LMT}} = 121$ A for $i = 31, \ldots, 55$. The nominal output voltage is 480 V AC, line to line. Then, $|V| = 480/\sqrt{3} = 277.1$ V.

Let us consider the condition that all the solar panels in the system have same solar irradiation level. The solar irradiation profile we employed in the simulation is shown in Fig. 3, which provides the solar irradiation of 8 hours during a day. From $t = 2\ h$ to $t = 5\ h$, it becomes cloudy such that the solar irradiation level is lower than it under a clear condition. The entire solar profile is noisy with a small random noise added. For such a given solar irradiation profile, we compare the algorithm based on optimal reactive power allocation strategy with two algorithms based on an evenly distributed reactive power allocation strategy.

The first algorithm is so-called *flexible even distribution* of the reactive power:

1. The reactive power demand of the grid is evenly divided into m parts, and each part is Q_D/m.
2. If $\max_i\{Q_i^{\min}\} <= Q_D/m <= \min_i\{Q_i^{\max}\}$, then the reactive power of each inverter is Q_D/m.
3. If the amount of reactive power Q_D/m exceeds the limits of some inverters, then for these inverters, the reactive power equals the limit (i.e., upper limit if $Q_D > 0$, lower limit if $Q_D < 0$); other inverters will evenly allocate the remaining reactive power demand.

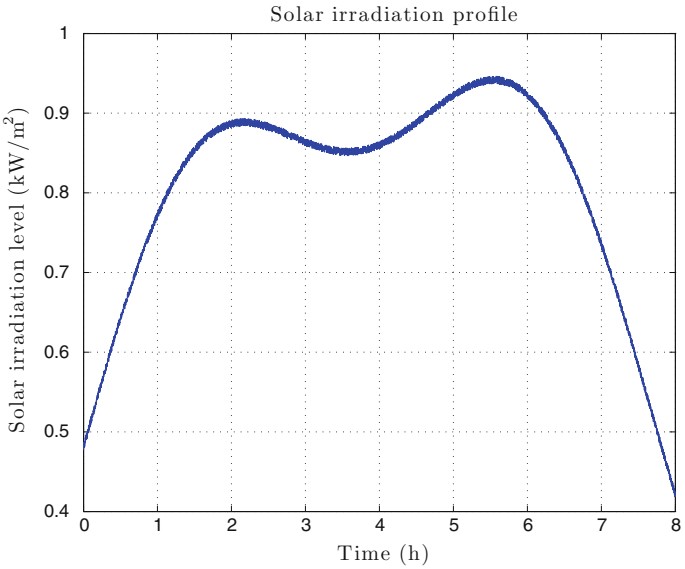

Fig. 3 Solar irradiation profile

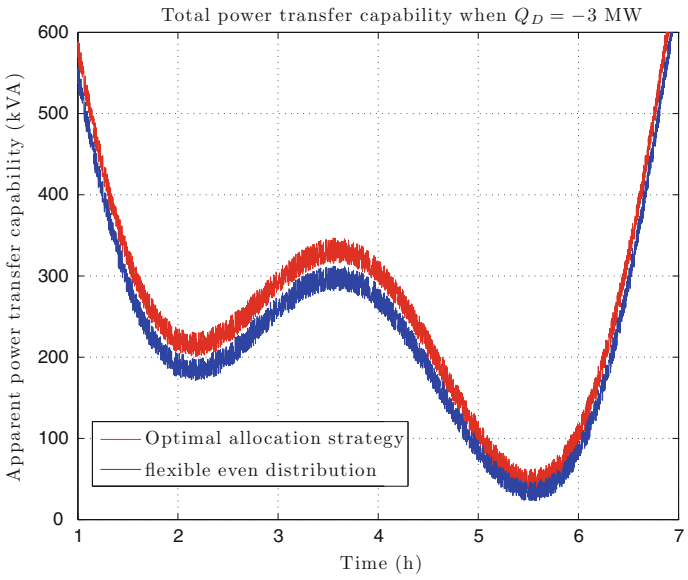

Fig. 4 Total power transfer capability: shown from $t = 1$ h to $t = 7$ h, expressed in kVA. The *top curve* is the power transfer capability for the optimal allocation algorithm, and the *bottom one* is for the *flexible even distribution* algorithm

In the simulation, we set the reactive power demand of the grid to be $Q_D = -3$ MW. The total power transfer capability obtained from simulation for the algorithm based on optimal allocation strategy and the *flexible even distribution* allocation algorithm is shown in Fig. 4. We observe from Fig. 4 that the optimal allocation algorithm

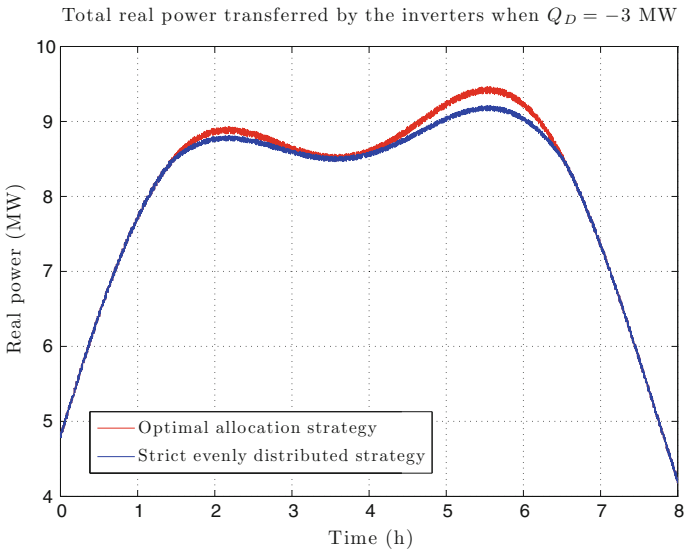

Fig. 5 Total active power transferred. The *top curve* is for the optimal allocation algorithm, and the *bottom one* is for the *strict even distribution* algorithm

is capable of transferring more power than the *flexible even distribution* algorithm. The *flexible even distribution* algorithm indicates that if the reactive power of some inverters reaches the limits, then other inverters will take more reactive power.

Next, we will compare the algorithm for the optimal allocation strategy with the so-called *strict even distribution* algorithm. For the *strict even distribution* algorithm, each inverter takes exactly Q_D/m of reactive power. The inverters of which the reactive power reaches the limits do not allocate extra reactive power on other inverters, but sacrifice certain amount of transferred active power instead. For a solar profile given in Fig. 3, the total transferred active power for both algorithms is shown in Fig. 5. It is obvious that the optimal allocation strategy algorithm transfers more active power than the *strict even distribution* algorithm when the solar irradiation level is high. It is worth pointing out that the total power transfer capability of the *strict even distribution* algorithm is higher than the one of the optimal allocation strategy algorithms at some points. However, it is because that the *strict even distribution* algorithm sacrifices much active power instead.

5 Conclusions

Based on the power capability function we defined for the grid-connected PV systems with multiple DC–AC inverters, we proposed the optimal allocation strategies for the case that no inverter's reactive power reaches the limits when the reactive power demand is small, and for the case that some inverters' reactive powers reach their limits when the reactive power demand is large. We have provided the analytical solution of the reactive power allocation strategies. Moreover, we mathematically proved the

strategies are optimal. In order to seek the inverters with reactive power that hits its limits, an order has been used to sort all the DC–AC inverters for the identification. Finally, we introduced an algorithm based on the optimal allocation strategy and compared such an algorithm with two other algorithms to show its optimality in a case study. One possible future direction is to develop the control schemes for the optimal allocation strategies we proposed here and apply the control techniques in simulation or for real systems.

Appendix: Proofs of Theorems and Lemmas

Proof of Theorem 3.1 Here, we use Lagrange multiplier method [17] to solve the problem given in (6) and only consider the positive part. Let $Q = \left[Q_1, \ldots, Q_m\right]^{\mathrm{T}}$, the Lagrangian function is constructed as follows,

$$\begin{aligned} L(Q, \lambda, \mu) = &- \sum_{i=1}^{m} \left(C_i^{\mathrm{LMT}} - \frac{\sqrt{P_i^2 + Q_i^2}}{3|V|} \right) + \lambda \left(\sum_{i=1}^{m} Q_i - Q_D \right) \\ &+ \sum_{i=1}^{m} \mu_i \left(Q_i - \sqrt{9|V|^2 \left(C_i^{\mathrm{LMT}}\right)^2 - P_i^2} \right) \end{aligned} \tag{15}$$

where λ, μ_j, $j = 1, \ldots, m$ are Lagrange multipliers. As for this case we assume the reactive power of the ith inverter Q_i satisfies (5) with strictly inequalities, the inequality constraints are inactive. Hence, the Lagrangian function in (15) becomes

$$L(Q, \lambda) = - \sum_{i=1}^{m} \left(C_i^{\mathrm{LMT}} - \frac{\sqrt{P_i^2 + Q_i^2}}{3|V|} \right) + \lambda \left(\sum_{i=1}^{m} Q_i - Q_D \right) \tag{16}$$

Let the gradient of the Lagrangian function (16) $\nabla_Q L(Q, \lambda) = 0$, we have

$$\frac{Q_i}{3|V|\sqrt{P_i^2 + Q_i^2}} = -\lambda, i = 1, \ldots, m \tag{17}$$

From (17), we know that Q_i and λ have opposite signs, and $|V|$ and P_i are both positive, so we obtain

$$Q_i = -\frac{3|V|P_i\lambda}{\sqrt{1 - 9|V|^2\lambda^2}} \tag{18}$$

If we substitute (18) into $\sum_{i=1}^{m} Q_i = Q_D$, we obtain one equation with λ as the only variable,

$$-\frac{3|V|P_i\lambda}{\sqrt{1 - 9|V|^2\lambda^2}} \sum_{i=1}^{m} P_i - Q_D = 0 \tag{19}$$

By solving (19), we have

$$\lambda^2 = \frac{Q_D^2}{9|V|^2\left((\sum_{i=1}^m P_i)^2 + Q_D^2\right)}$$

As Q_i and λ have opposite signs, it is obvious that Q_D and λ also have opposite signs. Then, λ is expressed as follows,

$$\lambda = -\frac{Q_D}{3|V|\sqrt{(\sum_{i=1}^m P_i)^2 + Q_D^2}} \tag{20}$$

Substituting (20) in (17), we have the reactive power Q_i^*, $i = 1, \ldots, m$,

$$Q_i^* = \frac{P_i}{\sum_{i=1}^m P_i} Q_D, i = 1, \ldots, m \tag{21}$$

To guarantee Q_i^* in (21) is the optimal reactive power for the ith inverter, and we need to the Hessian of the Lagrangian function to be positive definite [17]. The Hessian of the Lagrangian function is

$$\nabla_{QQ} L(Q^*, \lambda^*) = \begin{bmatrix} \frac{P_1^2}{3|V|\left(P_1^2+Q_1^2\right)^{3/2}} & 0 & \cdots & 0 \\ 0 & \frac{P_2^2}{3|V|\left(P_2^2+Q_2^2\right)^{3/2}} & \cdots & 0 \\ \vdots & \vdots & \ddots & \vdots \\ 0 & 0 & \cdots & \frac{P_m^2}{3|V|\left(P_m^2+Q_m^2\right)^{3/2}} \end{bmatrix}$$

where λ^* is the one given in (20). For all $y \neq 0$ such that $\nabla(\sum_{i=1}^m Q_i - Q_D)^{\mathrm{T}} y = 0$, we have

$$y^{\mathrm{T}} \nabla_{QQ} L\left(Q^*, \lambda^*\right) y = \sum_{i=1}^m \frac{P_i^2}{3|V|\left(P_i^2 + Q_i^2\right)^{3/2}} y_i^2 > 0$$

Hence, the Hessian of the Lagrangian function is positive definite. So Q_i^* given by (21) is the optimal reactive power profile. To let the inactive inequalities assumption hold, we need Q_i^* to satisfy the first inequality of (5) (for positive Q_i). Then, we have

$$\frac{P_i}{\sum_{i=1}^m P_i} Q_D \leq \sqrt{9|V|^2\left(C_i^{\mathrm{LMT}}\right)^2 - P_i^2}, \; i = 1, \ldots, m \tag{22}$$

As (22) needs to hold for all inverters, we obtain

$$Q_D \leq \min_{i=1,\ldots,m} \left\{ \frac{\sqrt{9|V|^2\left(C_i^{\mathrm{LMT}}\right)^2 - P_i^2}}{P_i} \sum_{i=1}^m P_i \right\}$$

for positive Q_i, similarly we can prove the negative part, which proves (8). □

Proof of Lemma 3.1 Suppose that all the inverters are already sorted in the order given by (10) and in such an order the reactive power of the first $r-1$ inverters already hit their upper bounds. Now consider the assumption that the reactive power of the rth inverter does not reach its upper bound, i.e., $Q_r < Q_r^{\max}$, and the reactive power of the $(r+1)$th inverter hits its upper bound, i.e., $Q_{r+1} = Q_{r+1}^{\max}$. As indicated by the assumption, the reactive powers Q_r and $Q_i, i = r+2, \ldots, m$, do not hit their upper bounds, and according to Theorem 3.1 for these $m-r$ reactive powers, we have

$$Q_i = \frac{Q_D - \sum_{i=1}^{r-1} Q_i^{\max} - Q_{r+1}^{\max}}{\sum_{i=1}^{m} P_i - \sum_{i=1}^{r-1} P_i - P_{r+1}} P_i, \ i = r, r+2, \ldots, m \tag{23}$$

For the rth inverter, we substitute (23) into $Q_r < Q_r^{\max}$, then we have

$$\frac{Q_D - \sum_{i=1}^{r-1} Q_i^{\max} - Q_{r+1}^{\max}}{\sum_{i=1}^{m} P_i - \sum_{i=1}^{r-1} P_i - P_{r+1}} P_r < Q_r^{\max} \tag{24}$$

The $(r+1)$th inverter's reactive power Q_{r+1}, by the assumption, hits the upper bounds. If we apply Theorem 3.1 and calculate Q_{r+1} by using a manner similar to (23), the reactive power Q_{r+1} will exceed the upper bound $Q_{r+1}^{\max}$. Based on this, we have such inequality

$$\frac{Q_D - \sum_{i=1}^{r-1} Q_i^{\max}}{\sum_{i=1}^{m} P_i - \sum_{i=1}^{r-1} P_i} P_r \geq Q_{r+1}^{\max} \tag{25}$$

As $P_i > 0, i = 1, \ldots, m$, from (24) and (25) we obtain

$$\frac{Q_D - \sum_{i=1}^{r-1} Q_i^{\max} - Q_{r+1}^{\max}}{\sum_{i=1}^{m} P_i - \sum_{i=1}^{r-1} P_i - P_{r+1}} < \frac{Q_r^{\max}}{P_r} \tag{26}$$

and

$$\frac{Q_D - \sum_{i=1}^{r-1} Q_i^{\max}}{\sum_{i=1}^{m} P_i - \sum_{i=1}^{r-1} P_i} \geq \frac{Q_{r+1}^{\max}}{P_{r+1}} \tag{27}$$

Subtract the left-hand side of (26) by the left-hand side of (27), we obtain the following inequality

$$\begin{aligned} &\frac{Q_D - \sum_{i=1}^{r-1} Q_i^{\max} - Q_{r+1}^{\max}}{\sum_{i=1}^{m} P_i - \sum_{i=1}^{r-1} P_i - P_{r+1}} - \frac{Q_D - \sum_{i=1}^{r-1} Q_i^{\max}}{\sum_{i=1}^{m} P_i - \sum_{i=1}^{r-1} P_i} \\ &= \frac{(Q_D - \sum_{i=1}^{r-1} Q_i^{\max}) P_{r+1} - (\sum_{i=1}^{m} P_i - \sum_{i=1}^{r-1} P_i) Q_{r+1}^{\max}}{(\sum_{i=1}^{m} P_i - \sum_{i=1}^{r-1} P_i - P_{r+1})(\sum_{i=1}^{m} P_i - \sum_{i=1}^{r-1} P_i)} \geq 0 \end{aligned} \tag{28}$$

The reason that (28) holds is that from (25) we know

$$\left(Q_D - \sum_{i=1}^{r-1} Q_i^{\max}\right) P_{r+1} \geq \left(\sum_{i=1}^{m} P_i - \sum_{i=1}^{r-1} P_i\right) Q_{r+1}^{\max}$$

and the denominator of the second line of (28) is obviously positive. Hence,

$$\frac{Q_D - \sum_{i=1}^{r-1} Q_i^{\max} - Q_{r+1}^{\max}}{\sum_{i=1}^{m} P_i - \sum_{i=1}^{r-1} P_i - P_{r+1}} \geq \frac{Q_D - \sum_{i=1}^{r-1} Q_i^{\max}}{\sum_{i=1}^{m} P_i - \sum_{i=1}^{r-1} P_i} \tag{29}$$

From (25), (26), and (29), we have the following inequality,

$$\frac{Q_r^{\max}}{P_r} > \frac{Q_D - \sum_{i=1}^{r-1} Q_i^{\max} - Q_{r+1}^{\max}}{\sum_{i=1}^{m} P_i - \sum_{i=1}^{r-1} P_i - P_{r+1}} \geq \frac{Q_D - \sum_{i=1}^{r-1} Q_i^{\max}}{\sum_{i=1}^{m} P_i - \sum_{i=1}^{r-1} P_i} \geq \frac{Q_{r+1}^{\max}}{P_{r+1}} \tag{30}$$

The inequality in (30) shows $\frac{Q_r^{\max}}{P_r} > \frac{Q_{r+1}^{\max}}{P_{r+1}}$ which contradicts the order in (10). Hence, the assumption that $Q_r < Q_r^{\max}$, while $Q_{r+1} = Q_{r+1}^{\max}$ is invalid. Then, we conclude that when $Q_D > 0$ the first r inverters' reactive power Q_i, $i = 1, \ldots, r$ in the order given in (10) hit their upper bounds. For the rest $m - r$ inverters, the following inequality holds,

$$\frac{P_i}{\sum_{i=r+1}^{m} P_i}\left(Q_D - \sum_{i=1}^{r} Q_j^{\max}\right) < Q_i^{\max},\ i = r+1, \ldots, m \tag{31}$$

Thus, r is the minimum number that makes (31) hold. □

Proof of Theorem 3.2 We use Lagrange multiplier method [17] to prove this theorem. The Lagrangian function is the one given in (15). We have two cases. The reactive power demand $Q_D > 0$. For this case, all the inverters are in the order given in (10). By Lemma 3.1, we know that those r inverters with reactive power that hits the upper bound are the first r inverters in that order. Hence, the inequality constraints

$$g_i(Q_i) = Q_i - \sqrt{9|V|^2 \left(C_i^{\mathrm{LMT}}\right)^2 - P_i^2} \leq 0,\ i = 1, \ldots, r$$

are active. For $i = 1, \ldots, r$, we have

$$Q_i = Q_i^{\max},\ i = 1, \ldots, r \tag{32}$$

and by taking the gradient of (15) we have

$$\mu_i = -\frac{Q_i}{3|V|\sqrt{P_i^2 + Q_i^2}} - \lambda,\ i = 1, \ldots, r \tag{33}$$

For those $m - r$ inverters with inactive inequality constraints, we have

$$\frac{Q_i}{3|V|\sqrt{P_i^2 + Q_i^2}} + \lambda = 0,\ i = r+1, \ldots, m \tag{34}$$

Also, we have the equality constraints which we are

$$\sum_{i=1}^{r} Q_i + \sum_{i=r+1}^{m} Q_i - Q_D = 0 \tag{35}$$

From (34), we obtain,

$$Q_i = -\frac{3|V|P_i\lambda}{\sqrt{1 - 9|V|^2\lambda^2}},\ \text{for } i = r+1, \ldots, m \tag{36}$$

Substitute (32) and (36) in (35), and we obtain

$$\begin{aligned}
&\sum_{i=1}^{r} Q_i - \frac{3|V|\lambda}{\sqrt{1 - 9|V|^2\lambda^2}} \sum_{i=r+1}^{m} P_i - Q_D = 0 \\
&\frac{3|V|\lambda}{\sqrt{1 - 9|V|^2\lambda^2}} = -\frac{Q_D - \sum_{i=1}^{r} Q_i}{\sum_{i=r+1}^{m} P_i} \\
&9|V|^2\lambda^2\left(\sum_{i=r+1}^{m} P_i\right)^2 = \left(Q_D - \sum_{i=1}^{r} Q_i\right)^2 \left(1 - 9|V|^2\lambda^2\right) \\
&9|V|^2\lambda^2\left(\left(\sum_{i=r+1}^{m} P_i\right)^2 + \left(Q_D - \sum_{i=1}^{r} Q_i\right)^2\right) = \left(Q_D - \sum_{i=1}^{r} Q_i\right)^2
\end{aligned} \tag{37}$$

From the second line of (37), we know that λ has the opposite sign of $Q_D - \sum_{i=1}^{r} Q_i$. In this case, λ is negative. As $Q_i = Q_i^{\max}$, $i = 1, \ldots, r$. Hence,

$$\lambda = -\frac{Q_D - \sum_{i=1}^{r} Q_i^{\max}}{3|V|\sqrt{(\sum_{i=r+1}^{m} P_i)^2 + (Q_D - \sum_{i=1}^{r} Q_i^{\max})^2}} \tag{38}$$

Substitute (32) and (38) in (36), and we obtain (12).

For this case,

$$\mu_j > 0,\ \forall j \in A(Q) \tag{39}$$

where $A(Q) = \{j \mid g_j(Q) = 0\}$ is the index set that the inequality constraints are active. Now we show the reason why (39) holds. We assume some inverters' reactive powers hit their upper bounds, (8) does not hold. Then, consider the inverters in the order given by (10). For $i = 1, \ldots, r$, $Q_i = Q_i^{\max}$, then

$$Q_i^{\max} < \frac{P_i}{\sum_{i=1}^m P_i} Q_D,\ i = 1, \ldots, r$$

The reactive power Q_i, $i = 1, \ldots, r$, reaches its upper bound, so the amount of reactive power $\frac{P_i}{\sum_{i=1}^m P_i} Q_D - Q_i^{\max}$, $i = 1, \ldots, r$, will be allocated on other inverters. Hence,

$$Q_j \geq \frac{P_i}{\sum_{i=1}^m P_i} Q_D,\ j = r+1, \ldots, m \tag{40}$$

Then, we obtain

$$\frac{Q_i^{\max}}{P_i} < \frac{Q_j}{P_j},\ i = 1, \ldots, r,\ j = r+1, \ldots, m \tag{41}$$

From (33) and (38), μ_i^* is expressed as

$$\begin{aligned} \mu_i^* = & \frac{Q_D - \sum_{i=1}^r Q_i^{\max}}{3|V|\sqrt{\left(\sum_{i=r+1}^m P_i\right)^2 + \left(Q_D - \sum_{i=1}^r Q_i^{\max}\right)^2}} \\ & - \frac{Q_i^{\max}}{3|V|\sqrt{P_i^2 + \left(Q_i^{\max}\right)^2}},\ i = 1, \ldots, r \end{aligned} \tag{42}$$

Since $Q_D - \sum_{i=1}^r Q_i^{\max} > 0$ and $Q_i^{\max} > 0$, we can turn (42) into the following form,

$$\mu_i^* = \frac{1}{3|V|\sqrt{\left(\frac{\sum_{i=r+1}^m P_i}{Q_D - \sum_{i=1}^r Q_i^{\max}}\right)^2 + 1}} - \frac{1}{3|V|\sqrt{\left(\frac{P_i}{Q_i^{\max}}\right)^2 + 1}},\ i = 1, \ldots, r \tag{43}$$

Now consider the denominators of those two terms in (43). From (12), we know that

$$\frac{P_j}{Q_j} = \frac{\sum_{i=r+1}^m P_i}{Q_D - \sum_{i=1}^r Q_i^{\max}},\ j = r+1, \ldots, m$$

From (41), we know that

$$\frac{P_j}{Q_j} < \frac{P_i}{Q_i^{\max}}$$

Hence, in (43) the denominator of the first term is smaller than the denominator of the second term. Then, we conclude that $\mu_j > 0, \forall j \in A(Q)$. For all $y \neq 0$ such that $\nabla h(Q)^{\mathrm{T}} y = 0$, and $\nabla g_j(Q)^{\mathrm{T}} y = 0, \forall j \in A(Q)$, we have

$$\nabla_{QQ} L(Q^*, \lambda^*, \mu^*) = \begin{bmatrix} \frac{P_1^2}{3|V|\left(Q_1^2+P_1^2\right)^{3/2}} & 0 & \cdots & 0 \\ 0 & \frac{P_2^2}{3|V|\left(Q_2^2+P_2^2\right)^{3/2}} & \cdots & 0 \\ \vdots & \vdots & \ddots & \vdots \\ 0 & 0 & \cdots & \frac{P_m^2}{3|V|\left(Q_m^2+P_m^2\right)^{3/2}} \end{bmatrix} \tag{44}$$

and

$$y^{\mathrm{T}} \nabla_{QQ} L(Q^*, \lambda^*, \mu^*) y = \sum_{i=1}^{m} \frac{P_i^2}{3|V|\left(Q_i^2 + P_i^2\right)^{3/2}} y_i^2 > 0 \tag{45}$$

The Hessian of the Lagrangian function is positive definite. Hence, the reactive power profile given by (12) is the optimal allocation reactive power profile when (8) is not satisfied. □

References

1. Kundur, P.: Power System Stability and Control. McGraw-Hill Companies Inc, New York (1994)
2. Zhang, W., Li, F., Tolbert, L.M.: Review of reactive power planning: objectives, constraints, and algorithms. IEEE Trans. Power Syst. **22**(4), 2177–2186 (2007)
3. Renewables 2014: global status report: http://www.ren21.net
4. PV power plants 2013: industry guide: http://www.pv-power-plants.com/
5. Rivera, S., Kouro, S., Wu, B., Leon, J.I., Rodriguez, J., Franquelo, L.G.: Cascaded H-bridge multilevel converter multistring topology for large-scale photovoltaic systems. In: Proceedings of 2011 IEEE International Symposium on Industrial Electronics. Gdansk, Poland (2011)
6. Rivera, S., Wu, B., Kouro, S., Wang, H., Zhang, D.: Cascaded H-bridge multilevel converter topology and three-phase balance control for large-scale photovoltaic systems. In: Proceedings of 2012 3rd IEEE International Symposium on Power Electronics for Distributed Generation Systems. Aalborg, Denmark (2012)
7. Agorreta, J.L., Borrega, M., Lopez, J., Marroyo, L.: Modeling and control of n-paralleled grid-connected inverters with LCL filter coupled due to grid impedance in PV plants. IEEE Trans. Power Electron. **26**(3), 770–785 (2011)
8. Borrega, M., Marroyo, L., Gonzalez, R., Balda, J., Agorreta, J.L.: Modeling and control of a master-slave PV inverter with n-paralleled inverters and three-phase three-limb inductors. IEEE Trans. Power Electron. **28**(6), 2842–2855 (2013)
9. Patel, H., Agarwal, V.: Maximum power point tracking scheme for PV systems operating under partially shaded conditions. IEEE Trans. Ind. Electron. **55**(4), 1689–1698 (2008)

10. Femia, N., Lisi, G., Petrone, G., Spagnuolo, G., Vitelli, M.: Distributed maximum power point tracking of photovoltaic arrays: novel approach and system analysis. IEEE Trans. Ind. Electron. **55**(7), 2610–2621 (2008)
11. Riffonneau, Y., Bacha, S., Barruel, F., Ploix, S.: Optimal power flow management for grid connected PV systems with batteries. IEEE Trans. Sustain. Energy **2**(3), 309–320 (2011)
12. IEEE Standard 1547^{TM}-2003. IEEE Std. Interconnecting Distributed Resources with Electric Power Systems (2003)
13. Smith, J.W., Sunderman, W., Dugan, R., Seal, B.: Smart inverter volt/var control functions for high penetration of PV on distribution systems. In: 2011 Power Systems Conference and Exposition (PSCE), Phoenix, AZ (2011)
14. Turitsyn, K., Sulc, P., Backhaus, S., Chertkov, M.: Options for control of reactive power by distributed photovoltaic generators. Proc. IEEE **99**(6), 1063–1073 (2011)
15. Cagnano, A., De Tuglie, E., Liserre, M., Mastromauro, R.A.: Online optimal reactive power control strategy of PV inverters. IEEE Trans. Ind. Electron. **58**(10), 4549–4558 (2011)
16. Xin, H., Qu, Z., Seuss, J., Maknouninejad, A.: A self-organizing strategy for power flow control of photovoltaic generators in a distribution network. IEEE Trans. Power Syst. **26**(3), 1462–1473 (2011)
17. Bertsekas, D.: Nonlinear Programming, 2nd edn. Athena Scientific, Belmont (1999)